DOI: 10.13009/EUCASS2022-4689
9TH EUROPEAN CONFERENCE FOR AERONAUTICS AND SPACE SCIENCES (EUCASS)

Progress in Aerodynamic Studies for CALLISTO - Reusable VTVL Launcher First Stage Demonstrator

Josef Klevanski[1], Bodo Reimann[2], Sven Krummen[3], Moritz Ertl[4], Tobias Ecker[5], Johannes Riehmer[6] and Etienne Dumont[7]

[1]DLR, Institute of Aerodynamics and Flow Technology, Supersonic and Hypersonic Technologies Department, Linder Hoehe, 51147 Cologne, Germany, Josef.Klevanski@dlr.de

[2]DLR, Institute of Aerodynamics and Flow Technology, Spacecraft Department, Lilienthalplatz 7, 38108, Braunschweig, Germany, Bodo.Reimann@dlr.de

[3]DLR, Institute of Space Systems, Robert Hooke-Str. 7, 28359 Bremen, Germany, Sven.Krummen@dlr.de

[4]DLR, Institute of Aerodynamics and Flow Technology, Spacecraft Department, Bunsenstr. 10, 37073 Gottingen, Germany, Moritz.Ertl@dlr.de

[5]DLR, Institute of Aerodynamics and Flow Technology, Spacecraft Department, Bunsenstr. 10, 37073 Gottingen, Germany, Tobias.Ecker@dlr.de

[6]DLR, Institute of Aerodynamics and Flow Technology, Supersonic and Hypersonic Technologies Department, Linder Hoehe, 51147 Cologne, Germany, Johannes.Riehmer@dlr.de

[7]DLR, Institute of Space Systems, Robert Hooke-Str. 7, 28359 Bremen, Germany, Etienne.Dumont@dlr.de

Abstract

Reusability applied to launchers is expected to reduce costs for access to space and to increase the operational flexibility. DLR, CNES and JAXA are jointly developing a vertical take-off and landing (VTVL) reusable subscaled first stage demonstrator with the objective to improve knowledge in this field. With this vehicle, called CALLISTO (Cooperative Action Leading to Launcher Innovation in Stage Toss back Operations), DLR, CNES and JAXA want to acquire and demonstrate the capability to launch, land and relaunch a vehicle under conditions representative for the first stage of an operational launch vehicle. Furthermore, during CALLISTO demonstration flights, data will be gathered to improve knowledge on the operation of a reusable vehicle which will help to optimize the reusability capabilities of future launch systems [1-2]. The entire CALLISTO reference mission is complex and includes many flight phases: ascent, boost-back manoeuvre, descent and landing during which the aerodynamic shape and the thrust level are changing radically. For instance, the simulation of the retro-propulsion plume is of particular importance, as it has a major impact on the base pressure distribution and aerothermal loads. In order to refine the requirements in preparation for the product preliminary design review (Product PDR), extensive aerodynamic analyses and tests have been performed [3-4]. The key challenge is to create an extensive aerodynamic data base covering all the flight configurations and conditions which than can be used for 6-DoF flight dynamics simulation, considering the complex aerodynamic shape of the demonstrator with limited computing resources. Indeed, the aerodynamic performance plays a central role in the global performance of CALLISTO. The use of classic engineering aerodynamic prediction methods cannot provide the precision and reliability necessary for the estimation of the aerodynamic coefficients. It is necessary to use a combination of models and CFD methods of different complexity. Another important aspect is the estimation of the uncertainties, based on the comparison of results calculated by different CFD methods as well as experimental results obtained in wind tunnels [5-7]. This paper will describe the concept and structure of the aerodynamic data base as well as the methods used for the calculation. The main findings of the aerodynamic analysis and the progress made during the CALLISTO project will be presented.

1. Introduction

The main goals of the implementation of reusability are to reduce the costs of access to space, and to increase the operation flexibility of launch vehicles. Further it may improve the reliability of space launches and solve the

DOI: 10.13009/EUCASS2022-4689

problem of utilization of used launch vehicle stages. The reuse of elements of launch vehicles has been the object of many research projects and studies in the past. The successes achieved in the recent years by Space X [8] and Blue Origin [9] in the reuse of the elements of space transportation systems based on the VTVL-concept have given new momentum in this area. To keep pace in the competitive international launch market. JAXA, CNES and DLR are working in close partnership to develop, build and fly the experimental reusable VTVL demonstrator called CALLISTO (Cooperative Action Leading to Launcher Innovation in Stage Toss-back Operations) [1] - [3]. The CALLISTO vehicle is a flight demonstrator for future reusable launcher stages and their technologies. The program involves three countries and their space organizations: CNES for France, DLR for Germany and JAXA for Japan. The first tests will be conducted in 2024 from CSG, Europe's Spaceport. The challenge is to develop, all along the project, the skills of the partners. This know-how includes products and vehicle design, ground segment set up, and post-flight operations for vehicle recovery then reuse. It should demonstrate the capability to recover and reuse a vehicle under conditions representative of a future operational launcher. This research project will allow developing, improving and testing the key technologies and knowledge necessary for the implementation of reusability. CALLISTO will perform several test- and demo-flights to demonstrate the capability to recover and reuse a vehicle under conditions representative of a future operational launcher and to gather the related experience.
After an successful Preliminary Design Review (PDR), the project has entered the detailed design phase for the launch system and its sub-systems [4]. Based on the identified need, additional outputs of the extended aerodynamic studies are:

- Estimation of the global aerodynamic coefficients CX, CY, CZ, CMx, CMy, CMz for the 6-DoF flight dynamics simulation and for the development of the GNC-System.
- Estimation of the local aerodynamic coefficients for structural load estimation and aerodynamic shape optimization.
- Estimation of the distributed aerodynamic loads: dCX/dX, dCY/dX, dCMZ/dX etc for structural load estimation.
- Evaluation of the thrust throttling impact on the aerodynamic characteristics.
- Evaluation of the plume deflection impact by Thrust Vector on the aerodynamic characteristics.
- Definition of the critical flight conditions

The main objectives are:

- Creation of the 6-Dof AErodynamic Data Base (AEDB) containing the aerodynamic function for the calculation of the forces and moments for all configurations, including estimated uncertainties
- Creation of the Aero-Thermodynamic Data Base (ATDB) containing the aerothermodynamic function for the calculation of the thermal loads for all configurations, including estimated uncertainties

The AEDB should also provide a continuous solution for the transition modes between the so-called base configurations. Therefore, special studies of the thrust throttling impact and of the thrust deflection impact on the aerodynamic were also performed and diverse transition functions were developed.

2. Mission analysis and flight configurations

The use of only one engine for a demonstration vehicle is very challenging, as the acceptable thrust to weight ratio has to be provided for start as well as for landing. It is much more difficult in comparison with launchers with multiple rocket engines like for example Falcon 9 with 9 engines. The available engine thrust with the minimum throttling ratio limits the start mass as well as the landing mass.
According to different limitations, the dynamic pressure along the trajectory is relatively high – in some cases too high to perform a tilt-over and boost-back manoeuvre relying on RCS (reaction and control system) thrusters only. As an alternative, the boost-back manoeuvre can be performed by deflection of the main engine with TVC while the engine is still running.

The primary mission objective is to demonstrate a so-called "toss-back" flight profile, which includes in particular the following phases:

- classic ascent phase (when compared to an expendable launch vehicle)
- attitude change phase, with tilt-over manoeuvre
- boost-back phase with targeting the landing site
- aerodynamic guided descent phase
- final landing boost and touchdown ("pin-point" landing)

DOI: 10.13009/EUCASS2022-4689

A candidate trajectory is shown in Figure 1. As an additional option, performing an ascent phase with the deployed, actively controlled fins is considered.

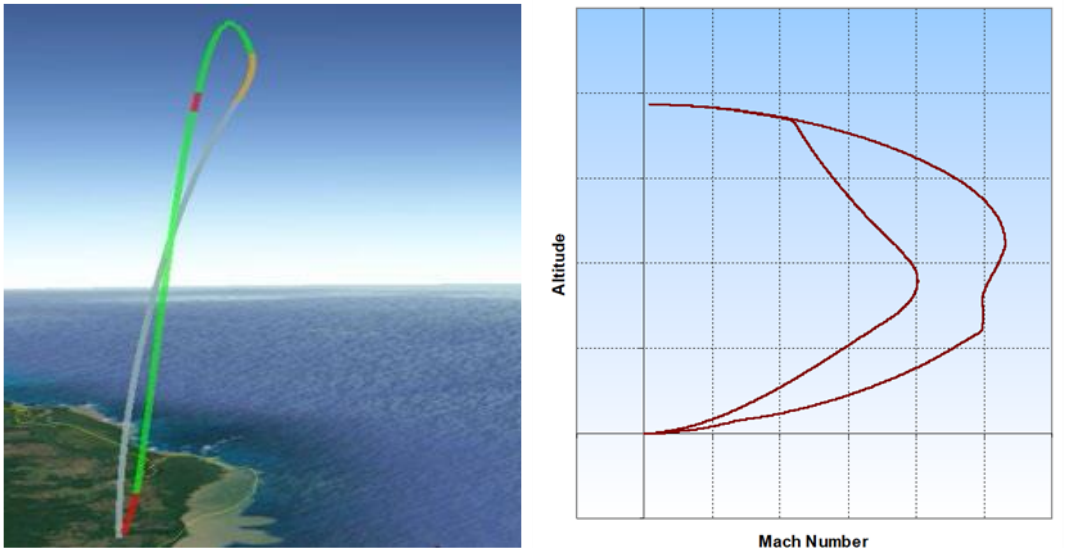

Figure 1: Candidate trajectory.

The nomenclature of the main flight configurations used in accordance with the demo flight phases (Configurations FFO – UUN) and the nomenclature of the additional flight configurations used for the test flights and for the transition between configurations is given in Table 1. Note that aerodynamic characteristics of the vehicle on the launch pad before launch is also the object of CFD computations (not presented here) and may influence the design of the CALLISTO system.

Table 1: CALLISTO flight configurations.

CONF	FFO	FFN	UFN	UFO	UUO	UUN	FUFN	FUFO	FUUO	FUO
Picture	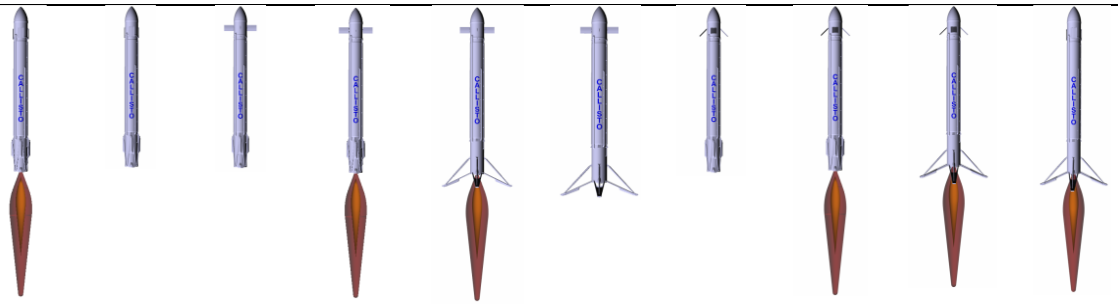									
Flight Phase	Ascent: MEIG#1 ↓ MECO#1	Ballistic: MECO#1 ↓ Fin Depl.	Ballistic & Aerodyn. Descent: Fin Depl. ↓ MEIG#2	Brake & Approach Boost: MEIG#2 ↓ Legs Deploy	Landing: Legs Depl. ↓ MECO#2 (Touch-down)	Landed (Park): After MECO#2	Transition: FFN ↓ UFN	Transition: FFO ↓ UFO	Transition: FUO ↓ UUO	Test Flights A, B
Fins	Folded	Folded	Unfolded	Unfolded	Unfolded	Unfolded	F→U	F→U	F→U	Folded
Land. Legs	Folded	Folded	Folded	Folded	Unfolded	Unfolded	Folded	Folded	Unfolded	Unfolded
Thrust Plume	Yes	No	No	Yes	Yes	No	No	Yes	Yes	Yes

In fact, on top of the reference flight profile, several flight profiles are under investigation in order to establish a consistent flight test plan which would enable the incremental increase of the difficulty of the flight up to the reference flight profile. Before the demo-flight this extensive incremental program of test flights is to be performed

DOI: 10.13009/EUCASS2022-4689

and therefore many additional configurations are also be analysed. The planned flight classes and the corresponding aerodynamic configurations are shown in Table 2:

Table 2: planned flight and corresponding aerodynamic configurations.

Flight Class	Configurations
Test Flight A	FUO
Test Flight B	FUO → UUO
Test Flight C	FFO → UFO → UUO
Test Flight D	FFO → FFN → UFN → UFO → UUO
Test Flight E (DEMO)	FFO → FFN → UFN → UFO → UUO
Test Flight E (Option)	UFO_ASC → UFN → UFO → UUO

Thus, the aerodynamic database of CALLISTO is very extensive: Mach number, altitude and dynamic pressure vary in a very broad range; the vehicle flies forwards in the ascent phase and rearwards in the approach and landing phases, during the tilt-over manoeuvre the angle of attack varies from 0 to 180°. Furthermore, the flight configuration changes for each flight phase: the aerodynamic control surfaces (fins) and landing legs are stowed during the ascent phase, the fins are then deployed for the aerodynamic descent phase. Finally, the landing legs are deployed shortly before the touch-down.
The trajectory was analysed to indicate the flight phases and configurations which are particularly important from an aerodynamic perspective. For each flight phase and configuration, the relative forces were compared: aerodynamic forces, thrust and RCS-forces. The results are shown in Figure 2. It can be seen that from aerodynamic point of view, the most important phase is the aerodynamically controlled descent, or in other words the flight configuration UFN.
The configuration FFN is not as critical as in this case the vehicle weight is largely dominating, but it shows the limitation of the RCS capabilities.
Both configurations UFN and UFO requires knowledge of the whole range of AoA = 0° to +180°.
In the case of FFO configuration, knowledge of aerodynamic characteristics and especially the drag is important for small angles of attack (AoA), in the range: -5° - +5°. For the FFN configuration in the culmination point the flight direction changes to the opposite, so the AoA varies in the range of AoA = 0° to +180°.

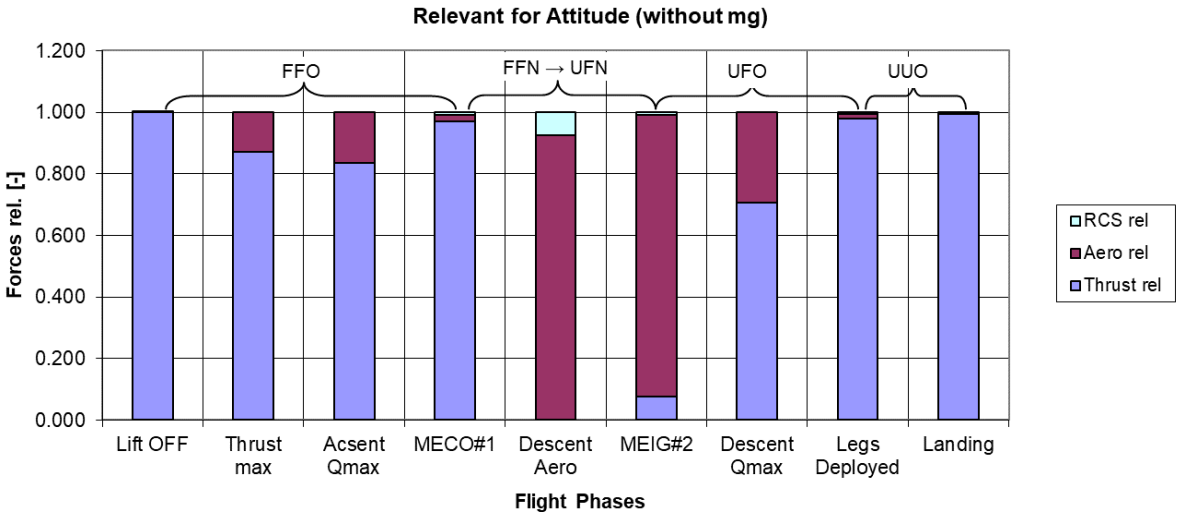

Figure 2: Comparative Analysis of the Forces & Moments: TVC, Aero, RCS.

3. Calculation strategy and reference frames

3.1 Calculation philosophy and applied methods

A philosophy, that has worked well in the pre-design phase, is used to create the extended databases. The philosophy and strategy of the aerodynamic study is presented in Figure 3 in the form of a "road-map". A simplified method and a High-Fidelity method were combined for the synthesis of the AEDB and ATDB. The results of the measurement

DOI: 10.13009/EUCASS2022-4689

campaigns carried out in wind tunnels were also used to validate and refine the databases. The special features and application of these methods are shortly described below.

Preliminary Aerodynamic Design Methods

The concept study during the preliminary design phase is important for the successful definition of the vehicle layout. Many aerodynamic computations should be performed in a short period of time with limited computational resources, in order to assess a large number of layouts. The so called "aero-prediction" codes, e.g., common estimation methods like Missile DATCOM can usually successfully be used for the preliminary design of missiles and launchers [11]. These methods are very fast and the preparation of the input data is relatively easy. These methods are very efficient for choosing the main design parameters (fuselage diameter, fin size etc.).

However, the analysis of the CALLISTO special features (wide range of Mach numbers, AoA = 0° to 180°, numerous flight configurations, thrust impact on the aerodynamics etc.) shows, that the strongly restricted domain of the successful application of the aero-prediction codes, cannot cover many application cases necessary for the reusable VTVL launchers. These codes are well suited for the calculation of the aerodynamic coefficients for launchers or missiles (typically simple revolution bodies) and for a limited range of the angle of attack. They are not well suited for complex aerodynamic shapes. The superposition principles used in these codes will not allow the precise calculation of the fin/fuselage interaction and the calculation of the distributed forces.

Therefore, CFD methods need to be applied in the current detailed design phase: CFD allows the aerodynamic calculations for subsonic as well as for transonic and supersonic regimes; for both simple and complex shapes. The CFD solver TAU in Euler mode (developed in DLR, see [13]) has already been used for the preliminary aerodynamic design. In this phase of extended aerodynamic calculations friction accounting was necessary; therefore, the CFD solver was used in the Navier-Stokes mode. The aerodynamic domain mesh was generated for each of the flight configurations identified in the computation matrix and for the reference fin deflections of -10°, 0°, +10°.

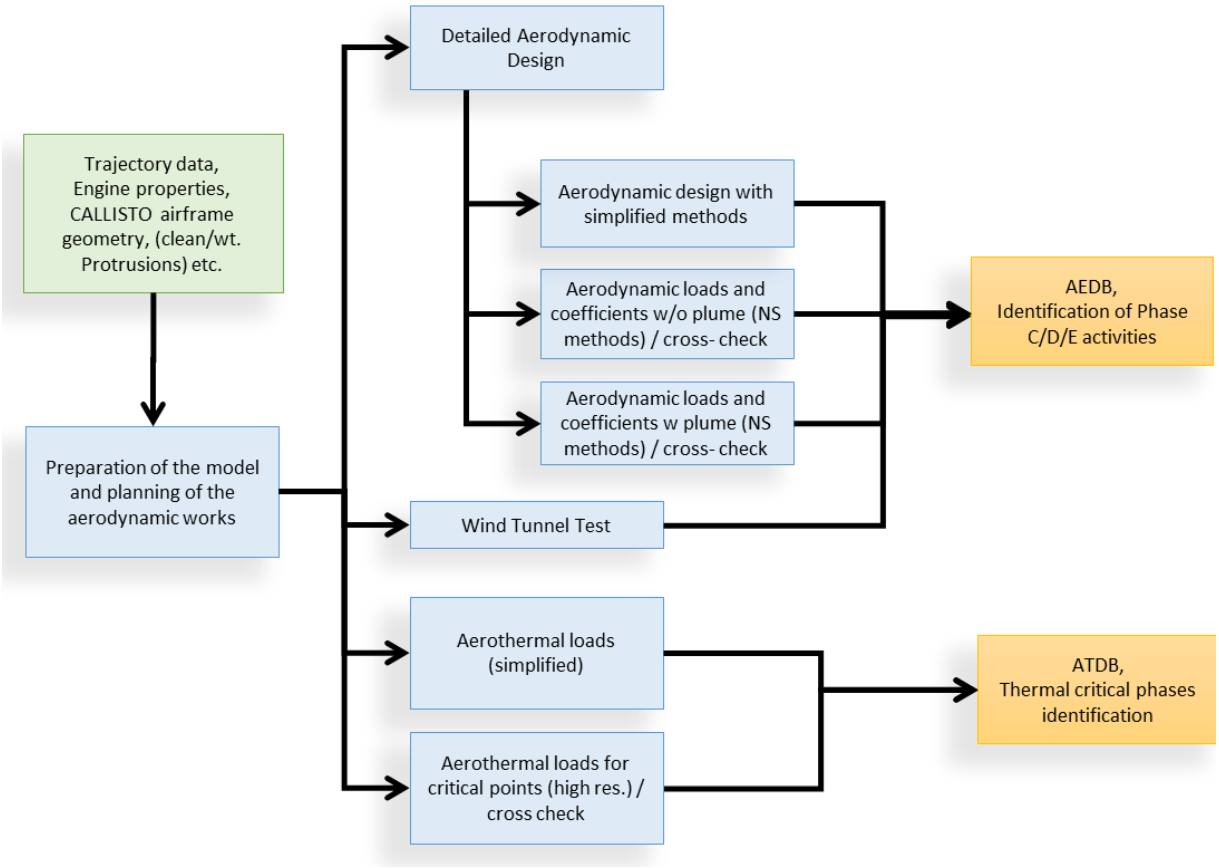

Figure 3. "Roadmap" for aerodynamic and aerothermodynamic studies.

The aerodynamic shape of the vehicle has become considerably more complex as a result of the further development of the design: numerous "superstructures" and protuberances such as cable ducts and external pipelines have now to

DOI: 10.13009/EUCASS2022-4689

be considered. The vehicle is not symmetric anymore; therefore, the use of the half-model to reduce the calculation time became impossible. In addition, the aerodynamic database should allow for 6-DoF flight dynamics simulations. This leads to the need to perform calculations not only in the AoA plane between 0° and 180° degrees, but also to repeat them for different roll angles. The volume of the calculation matrix is increasing to such an extent that creating an AEDB with High-Fidelity CFD alone in a short time and with limited computational resources becomes almost impossible. Usually, CFD methods require a very large amount of computational resources. In order to reduce the calculation time, the "Low-Fidelity" method the CFD solver used a coarse mesh with Navier-Stokes equations with very stable Spalart-Allmaras turbulence model [15]. The full-body domain was used for the all calculation – not only of the roll moments estimation.
All meshes were generated with the CENTAUR mesh generator [14] based on water-tight aerodynamic shapes (Figure 6, right). The same shapes were used also for the High-Fidelity aerodynamic computations in order to compare the results.
A two-gas mixture approach was used for the engine plume simulation, without simulation of chemical reactions, using standard air for the outer flow and an exhaust gas based on the products of the hydrogen-oxygen combustion.

High-Fidelity Aerodynamic Calculation
All High-Fidelity numerical investigations for the aerodynamic and aerothermal analysis of both ascent and descent flight were performed using the DLR flow solver TAU. The DLR TAU code is validated for a wide range of steady and unsteady sub-, trans-, super-, and hypersonic flow cases. Itis a second order finite-volume solver for the Euler and Navier-Stokes equations using eddy-viscosity, Reynolds-stress or detached and large eddy simulation for turbulence modelling. For the presented investigations, the Spalart-Allmaras one-equation eddy viscosity model [15] was used. The AUSMDV flux vector splitting scheme was applied together with MUSCL gradient reconstruction to achieve second order spatial accuracy. The applied model for thermodynamic and transport properties are based on a non-reacting mixture of thermally perfect gases (air and engine exhaust) and are derived from the CEA thermodynamic and transport databases. Detailed aerodynamic design performed by means of the High-Fidelity methods include:

- Calculation of the aerodynamic coefficients with the High-Fidelity tools (CFD: Navier-Stokes) for validation and tuning of the Low-Fidelity results
- Analysis of the aerodynamic flow for critical cases (including in particular plume effects during ascent, and retro-boosts)
- Analysis and validation of the calculated aerodynamic coefficients
- Evaluation of uncertainties
- Recommendations to vehicle on the aerodynamic and shape design
- Determination of pressure distribution
- 2D and 3D calculations of the aerothermal loads during the CALLISTO trajectory
- Analysis of the aerothermal loads for critical flight conditions (including in particular plume effects during ascent, and retro-boosts)
- Determination of heat flux distribution on specified thermal interfaces

Wind Tunnel Tests
In order to cross-check the CFD analysis and to evaluate the uncertainties, wind tunnel tests (WTT) were performed. They included the most critical configurations for both ascent and descent flight phases FFN and UFN. By the start of the test campaign, the first version of the CFD-based AEDB for FFN and UFN configurations had already been prepared. The modular models for the WTT are based on the same watertight aerodynamic shape which was used for the CFD analyses. The extended wind tunnel tests have been performed 2020 in the Trisonic Wind Tunnel (TMK-facility) of the DLR in Cologne and High-Speed Tunnel (HST) of the German-Dutch Wind-tunnels (DNW) in Amsterdam [10].

Main Results and Synthesis of the AEDB
All preliminary calculations of the aerodynamic coefficients were performed by means of CFD methods "Low-Fidelity" in Navier-Stokes mode. These calculations provided the results in the relative short time by use of the limited computational capabilities. The time necessary for computation of each configuration for a reference shape is 1-2 month on a typical workstation. However, the cross-check with the results gained by means of the High-Fidelity Navier-Stokes methods allows to calibrate the Low-Fidelity results and to tune the CFD parameters getting an adequate accuracy.
The High-Fidelity Navier-Stokes calculations provide the necessary accuracy but they require a large amount of computational resources and calculation time. For the most important configurations and flight regimes (ascent configuration FFO for AoA = ±10° and aerodynamically controlled descent configuration UFN, AoA = ±170°) the aerodynamic coefficients were calculated by use of the High-Fidelity Navier-Stokes methods.

DOI: 10.13009/EUCASS2022-4689

The performed wind tunnel tests results were used for the validation of the CFD results and for the estimation of the uncertainties primarily for the FFN and UFN configurations.

3.2 Choose of the reference frame for the AEDB

For creation of the AEDB the reasonable choice of the reference frame is extremely important. As mentioned above, the AEDB must allow the 6-DoF simulation of flight dynamics required for the development and validation of GNC. This means that the aerodynamic function must be able to calculate forces and moments at any attitude of the vehicle in relation to the airflow and must not have singular points; while the angle of attack varies between 0° and 180 °. For simulation of the 6-DoF flight dynamics, the body-fixed reference frame $OXYZ_f$ is normally used with the origin in the vehicle center of gravity CoG (Figure 4) reference frame to calculate aerodynamic coefficients as the basic coordinate system for the AEDB creation is inconvenient, as the coordinates of the CoG change significantly during the flight. To create the AEDB it is much more convenient to use the same reference frame that was used for the CFD calculations - $OXYZ_{TAU}$ with the origin coinciding with the fairing tip: this positioning of the origin ensures positive X-coordinate values over the entire length of the fuselage. This reference frame is connected with the CFD mesh. The positive direction of axes also conforms to the positive direction of CA, CN and CY of the Missile-DATCOM reference frame [11] solutions have been stored as TAU netcdf-files and as TAU-plot-files – with the same axes directions in TECPLOT-files and in TAU RAW Results – for global coefficients as well as for the distributed coefficients.

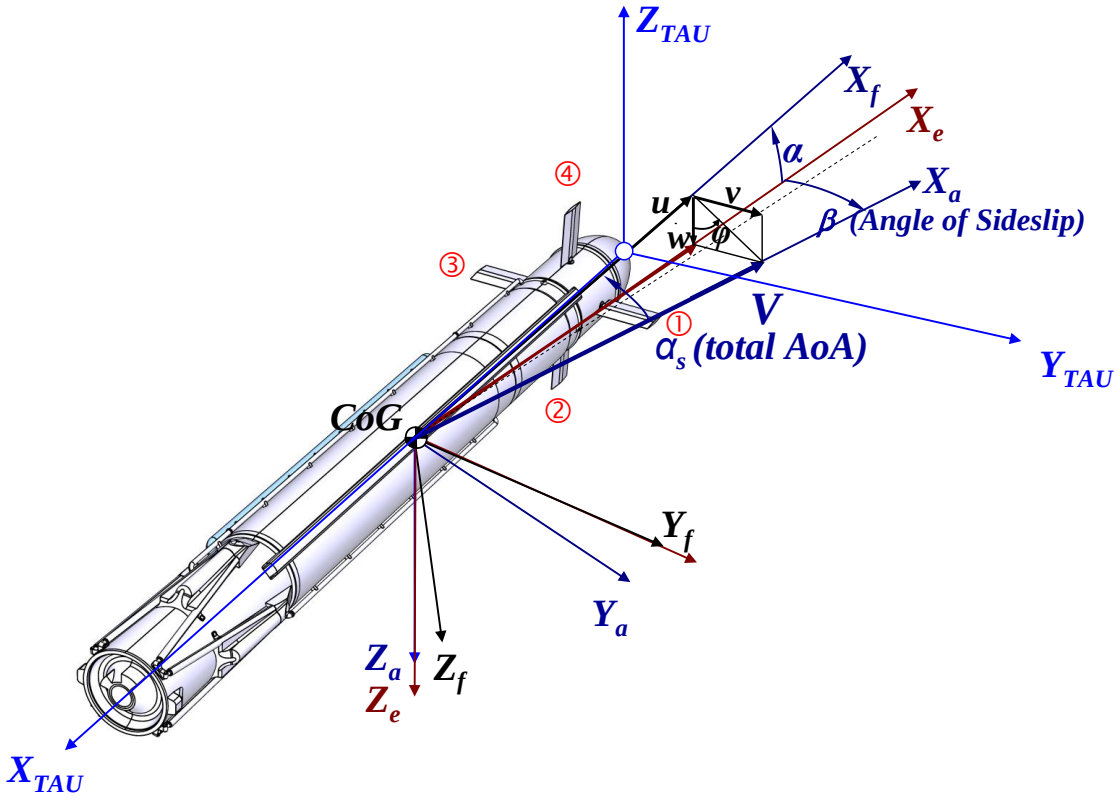

Figure 4: Reference Frames for CALLISTO.

The $OXYZ_{TAU}$ reference frame is also body-fixed and the aerodynamic forces and moments can be easily transformed into the reference frame $OXYZ_f$ later, during the flight dynamics simulation:

Translation: the transformation of a vector from $OXYZ_{TAU}$ to the $OXYZ_f$ requires a translation equivalent to the distance between the nose of the vehicle and the position of the vehicle Center of Mass (CoM) (origin of $OXYZ_f$) in TAU coordinates, i.e.,

$$r_{TAU}^{f} = \begin{bmatrix} X_{CoM} \\ Y_{CoM} \\ Z_{CoM} \end{bmatrix} \tag{3.1}$$

DOI: 10.13009/EUCASS2022-4689

Rotation: A rotation of 180° around Y_{TAU}-axis is needed to transform the TAU Axis System into the Body Reference frame, i.e.

$$A_{TAU}^{f} = \begin{bmatrix} -1 & 0 & 0 \\ 0 & 1 & 0 \\ 0 & 0 & -1 \end{bmatrix} \tag{3.2}$$

A convenient description of the three components of the flow velocity in relation to the vehicle is needed - unambigous and free from singularity in any flight direction and flow velocity. For the classical aeronautical approach (describing the aerodynamic flow by means of velocity V and angles α and β) the plane of change of angle of attack is being preferred, but this is only suitable for relatively small angles. However, for angles of attack and sliding angles close to 90° this description is not suitable.
To describe the direction of flow the use of velocity V, total angle of attack α_s and roll angle φ as input variables are much more convenient. It was proposed not to rotate the vehicle and the TAU-mesh, but simple rotate the stream direction. The total Angle of Attack α_s and the Angle of Rotation φ (Phi) will be transformed into α (AoA) and β (Angle of Sideslip) combination for CFD stream conditions:

$$\begin{aligned} u &= V \cdot \cos(\alpha_s) \\ v &= V \cdot \sin(\alpha_s) \cdot \sin(\varphi) \\ w &= V \cdot \sin(\alpha_s) \cdot \cos(\varphi) \\ \alpha &= \operatorname{atan2}(w,u) \\ \beta &= \operatorname{atan2}(v,\operatorname{sqrt}(u^2 + v^2)) \end{aligned} \tag{3}$$

So, the stream direction equivalent to the mesh rotation will be defined for the same body fixed axes, without risk of any transformation error. In Figure 5 the stream conditions are shown as a globe.Figure 5 the stream conditions are shown as a globe.
The stream conditions have been defined clearly and uniquely for each possible direction. The whole range of variation is defined for the roll angle Phi as -180° ≤ φ ≤ +180°, and for Alpha_s as 0° ≤ α_s ≤ 180°. Each stream direction can be estimated within the proposed range of variation. If Alpha_s is outside of this range, then both Alpha_s and Phi should be corrected.
Example: Alpha_s = 200° and Phi = 0° is equal to Alpha_s = 160° and Phi = 180°

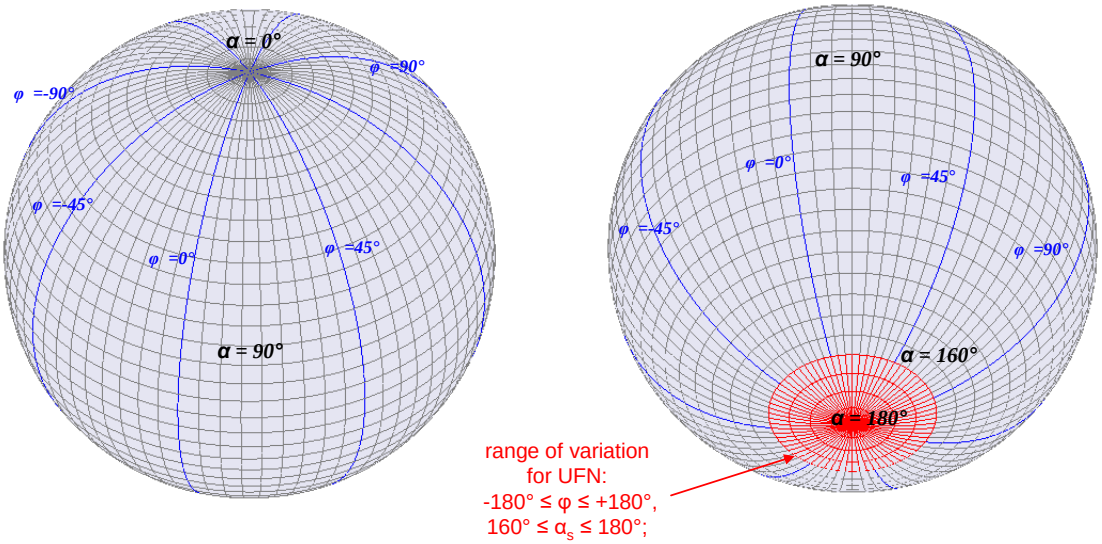

Figure 5: Globe of the stream conditions.

This unified approach is used to present the CFD-results and WTT-results as well as for the AEDB incorporating the aerodynamic function.

DOI: 10.13009/EUCASS2022-4689

4. Aeroshape evolution and local aerodynamics

Different vehicle layouts have been considered and analysed in the preliminary design phase. The development of the CALLISTO aerodynamic shape was accomplished with intensive aerodynamic studies: each layout was checked by extensive CFD simulations.
Whereas in the initial development phase of CALLISTO the aerodynamic team defined the aerodynamic shape of the vehicle and the structure designers had to realise it, in this phase of detailed development the aerodynamic a new task was given to the aerodynamic team: to assess the effect of the numerous design details on the aerodynamic performance compared to the ideal shape and to reduce the negative effects wherever possible.
The aerodynamic shape of the vehicle has become considerably more complex as a result of the further development of the design: numerous "superstructures" and protuberances such as cable ducts and external pipelines have appeared, the vehicle became not symmetric anymore (Figure 6).

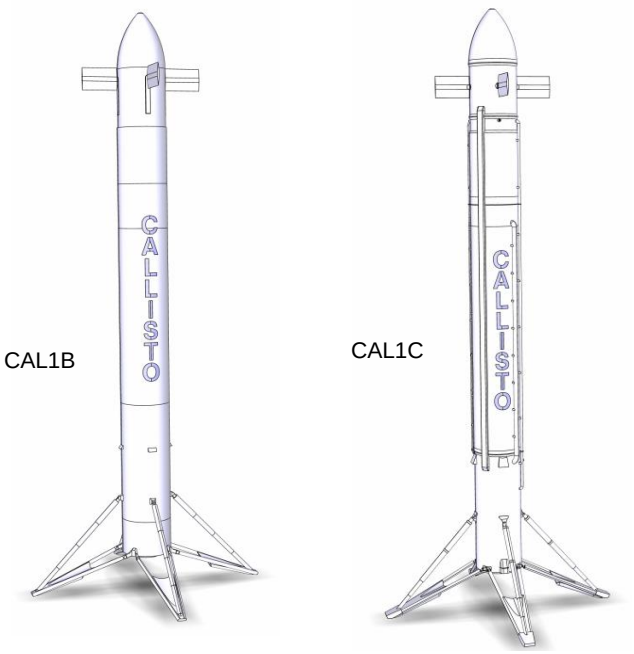

Figure 6. Aerodynamic shapes CAL1B and CAL1C.

4.1 L-Flange Design

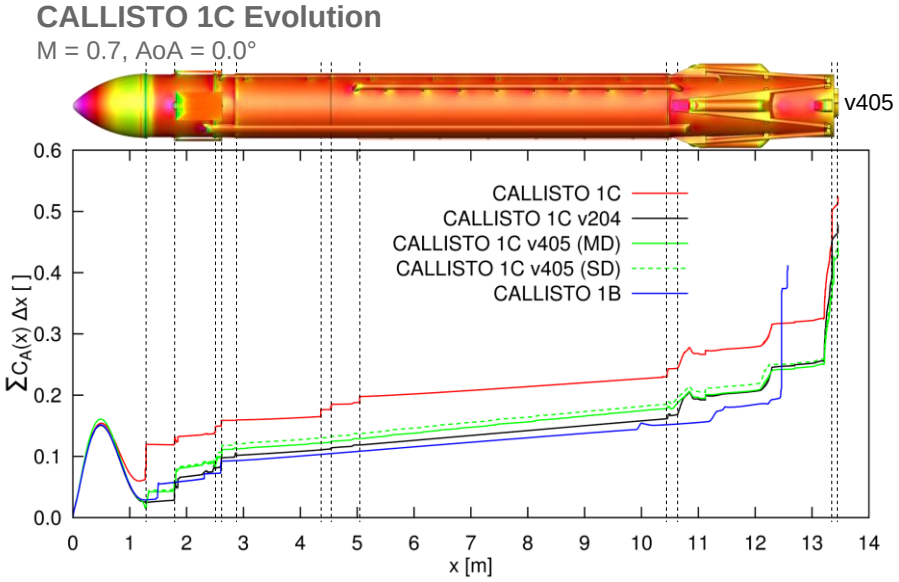

Figure 7: Impact of the Aeroshape evolution on the drag.

One of the first challenges was the assessment for the local aerodynamics: The structure design implied by the use of the so-called L-flanges for the reliable and easy connections for vehicle section. But the impact of the uncovered L-

DOI: 10.13009/EUCASS2022-4689

flanges led to very significant increase of the aerodynamic drag. The measures proposed by the aerodynamics team were the use of inclined ramps to improve the flow around the flanges. This local optimization has significantly reduced the negative effect of the L-Flanges, as can be seen in Figure 7.

5. Impact of the fins deflection and calculation of distributed loads

5.1 Impact of the fins deflection

A comparison of changes in global aerodynamic forces (acting on the whole vehicle) and local aerodynamic forces (acting only on the fin) obtained with CFD and WTT for configurations without and with a deflected fin, showed that the change in global aerodynamic forces is much greater than the change in local forces directly on the fin. This means that the aerodynamic interaction between the fin and the fuselage significantly increases the effect of fin deflection i.e. a simple superposition of forces on the fuselage and fin leads to a significant error.
Therefore, instead of using simple superposition, two other basic principles are used to calculate the deflection impact of the fin deflection for AEDB:

- Impact Superposition principle: The impact of the one fin deflection on the global aerodynamic coefficients and on the distributed load coefficients does not significantly affect the impacts of the other fin deflections, these impacts on the global coefficients (not on the local forces) can be superposed.
- Flow Similarity principle: The impact of the one fin deflection on the global aerodynamic coefficients and on the distributed load coefficients under certain flow conditions corresponds to the effect of deflection of any other fin under similar flow conditions.

In order to reduce the amount of calculations, the deflection effect was determined directly for fin #1 with deflection angles of -10°, 0° and +10° for whole range of the angles of attack and roll. A cyclic transformation of this effect was then used for the deflection of the fin#2, fin#3 and fin#4.
The same principles were used for the calculation of the distributed loads.

5.2 Distributed loads

Aerodynamic load distribution along the X-axis of the launcher is a very convenient way of representing many aspects:

- Check of the vehicle aerodynamics: Problematic positions can be identified.
- Optimizing and tuning of the CFD meshes
- Improvement of local aerodynamics
- Strength calculations: e.g., aerodynamic loads on fuselage beams

Distributed and local loads are often requested for the simulation of the actuators and deployment process, as well as for the determination of structural loads.

The basis for the calculation of distributed aerodynamic loads is the pressure distribution over the surface of the vehicle. As a rule, in addition to the pressure at the nodes of the aerodynamic grid, the aerodynamic forces and moments directly acting at these nodes are also contained. It is convenient to use these forces to calculate the loads distributed along the length. The basic principle in this approach is:

- The integrated coefficients are primary
- The distributed coefficients are secondary

The algorithm used is briefly described below:
The *n* knots for distribution are set with the constant step: $\Delta X = L/(n\text{-}1)$
The forces & moments from each original mesh knot *m* are redistributed between two nearest distribution knots *i* and *i+1*:

$$F_i = F_m \cdot (X_m - X_i)/\Delta X; \quad F_{i+1} = F_m \cdot (X_{i+1} - X_m)/\Delta X; \Rightarrow \quad \sum F_i + F_{i+1} \equiv F_m \tag{5.1}$$

All forces and moments collected in the distribution knots will be integrated (summed) and divided by $q \cdot S_{ref}$: they are the integrated coefficients. The integrated coefficient in the last distribution knot equals therefore exactly to the global coefficient.
The cubic spline based on the integrated coefficients will then be created. The analytic derivatives of this spline in the knots are the distributed coefficients. Thus, there are no discrepancies between global and distributed coefficients.

DOI: 10.13009/EUCASS2022-4689

The example of the distributed loads is shown in Figure 8.
As a result of the very limited computing resources and time, the basic calculations for all Mach numbers, angles of attack and roll angles were performed for the corresponding flight configuration either with undeflected fins or with only fin#1 deflected by -10° or by +10°. Extrapolation is strongly not recommended: It is associated with a high risk of non-physical results.
The processing still remains the same for forces and moments, for derivatives and for integrated coefficients.
The assumptions of superposition principle and similarity principle are best fulfilled in supersonic flight modes for both "+" and "x" configurations and in subsonic flight modes for the "+" configuration. For the "x" configuration at subsonic, these assumptions are not fully satisfied and the accuracy of the results is lower. Also, large angles of attack of the fin in relation to the flow (close or exceeding the angles of stall of the flow) essentially reduce the accuracy of the proposed method.

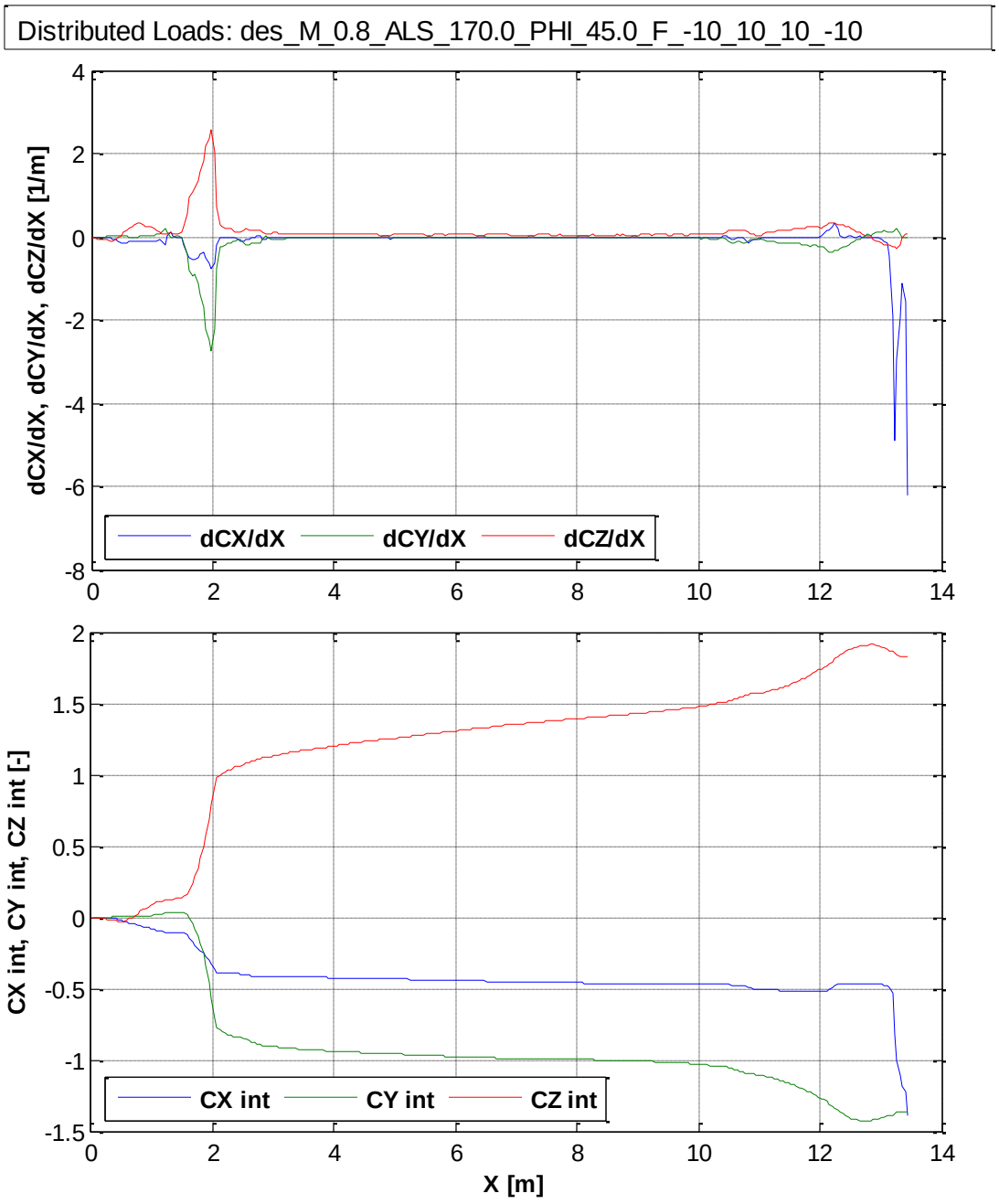

Figure 8: Distributed and integrated loads for the UFN-Configuration

DOI: 10.13009/EUCASS2022-4689

6. Thrust Impact on the Aerodynamics: Throttling, Gimbaling

6.1 Throttling Impact: Transition from aerodynamic data set UFN to aerodynamic set UFO

The analysis of the CFD results has shown that the change in aerodynamic characteristics, especially in drag during rearwards flight, with a change in thrust (engine throttling) has a substantially non-linear nature.
Therefore, a non-linear law proposed for a continuous (smooth) transition from one set of aerodynamic data UFN to another aerodynamic data set UFO as dependency of the relative thrust:

$$\text{if } t_{ST} < t < t_{ST} + T_{trans}: \; F_T = f(T_{rel}) \tag{6.1}$$

where:

- T_{rel} is the relative thrust: $T_{rel} = T/T_{100\%}$, $T_{100\%}$ = is defined for Sea Level conditions, possible values are between 0 and 1.1
- t [s] is the current simulation time
- t_{ST} [s] is the time of the transition beginning
- T_{trans} [s] is the duration of the transition
- $F_T(T_{rel})$ is the transition factor

The transition factor F_T was defined on basis of the High-Fidelity CFD calculations performed for M = 0.8, H = 5000 m, for UFN and UFO configurations with diverse engine modes and checked for other flight conditions (Figure 9).
The transition factor F_T depends on relative thrust T_{rel} and total angle of attack α_s with input limitation $0 \le T_{rel} \le 1.1$, $160° \le \alpha_s \le 180°$:
If necessary, the relative thrust T_{rel} can be easily calculated as a function of the mass flow by linear interpolation.

Estimation and use of the Transition Factor $F_T = f(T_{rel}, \alpha_s)$
The proposed approximation $F_T = f(T_{rel})$ well describes the transition from configuration UFN to UFO for $\alpha_s = 160…200°$.
The transition from the flight configuration UFN to the flight configuration UFO:

$$\begin{aligned}
CX(T_{rel}) &= CX_{UFN} \cdot (1 - F_T) + CX_{UFO} \cdot F_T; \\
CY(T_{rel}) &= CY_{UFN} \cdot (1 - F_T) + CY_{UFO} \cdot F_T; \\
CZ(T_{rel}) &= CZ_{UFN} \cdot (1 - F_T) + CZ_{UFO} \cdot F_T; \\
CMx(T_{rel}) &= CMx_{UFN} \cdot (1 - F_T) + CMx_{UFO} \cdot F_T; \\
CMy(T_{rel}) &= CMy_{UFN} \cdot (1 - F_T) + CMy_{UFO} \cdot F_T; \\
CMz(T_{rel}) &= CMz_{UFN} \cdot (1 - F_T) + CMz_{UFO} \cdot F_T;
\end{aligned} \tag{6.2}$$

This non-linear law provides a continuous (smooth) transition and can be applied for transition from UFN configuration to the UFO configuration. The time of the beginning of the transition t_{ST} should be indicated as transition event in the trajectory. The transition duration T_{trans} [s] should be defined for each kind of the configuration switching:

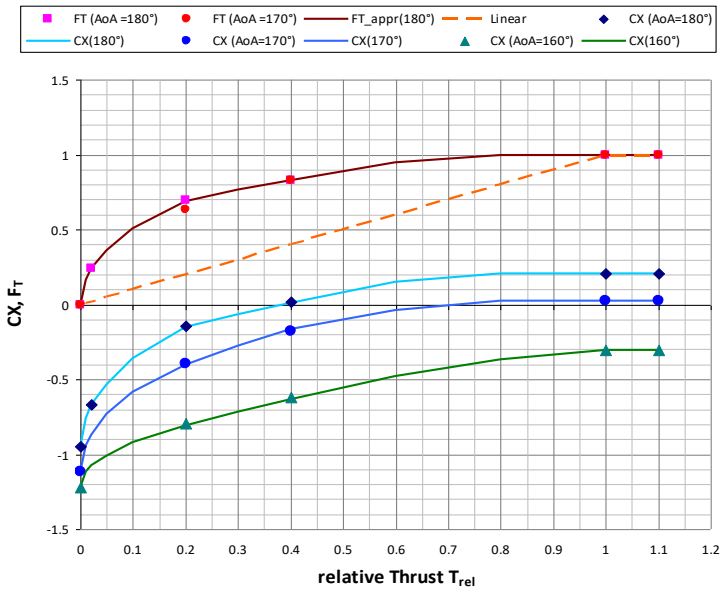

Figure 9: Estimation and use of the transition factor $F_T = f(T_{rel}, \alpha_s)$

DOI: 10.13009/EUCASS2022-4689

6.2 Thrust Deflection Impact (TVC-Impact) on the Aerodynamic

The Thrust Vector Control (TVC) via engine gimbaling is used by CALLISTO for attitude control during both ascent and descent phases. Especially in descent phase (retro propulsion phase) the strong impact of engine plume deflection onto the aerodynamic forces and moments is expected. The primary objectives of the performed study were the numerical evaluation of this impact and the development of the aerodynamic model extension for taking it into account for the flight simulation: the AEDB was originally defined for the undeflected engine plume.
The preliminary comparative analysis of the all forces acting on the vehicle determines the critical flight phases, where the aerodynamic forces are most significant (Figure 2):
The most critical flight phase for TVC-Impact on the aerodynamics is the descent phase in the UFO-configuration during which the engine is at full thrust and high dynamic pressures are present.
The numerous CFD-calculations with the engine thrust deflection were performed for the TVC-Impact Study for the reference flight conditions described below:

- High-Fidelity:
  - Configuration UFO, Thrust Level 20%, 40% 110%, TVC_q = 0°, 5°
  - Ma = 0.8, H = 5000 m, AoA = 160°, 170°, 175°, 180°
    AoA = 175°, AoR = 180° => AoA = 185°
- Low-Fidelity:
  - Configuration UFO, Thrust Level 100%, TVC_q = 0°, 3°, 5°, -5°
  - Ma = 0.8, H = 5000 m,
  - AoA = 160°, 165°, 160°, 170°,175°, 180°, 185°, 190° 195°, 200°
    AoR = 0°, 45°, 90°

where TVC_q is TVC deflection in XOZ-plane, sign rule is like Fin#1 and TVC_r is TVC deflection in XOY-plane.
A watertight model with moveable nozzle shown in Figure 10 was developed specifically for the TVC-impact study.

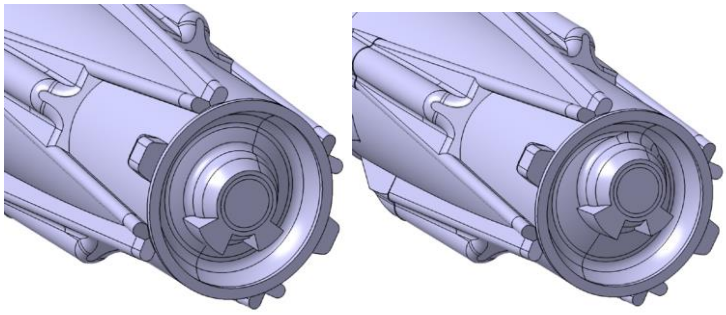

Figure 10: Special watertight model with moveable nozzle

An example of High-Fidelity CFD flow visualisations for different angle of attack with and without TVC deflection is shown in Figure 11.

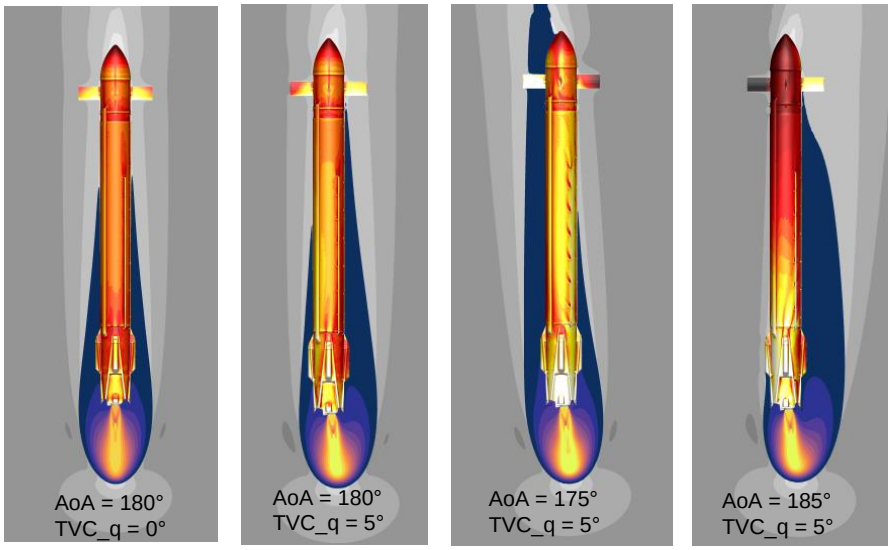

DOI: 10.13009/EUCASS2022-4689

Figure 11: CFD-Simulation without/with TVC-deflection

The results of the CFD-simulations are presented in Figure 12 and Figure 13.

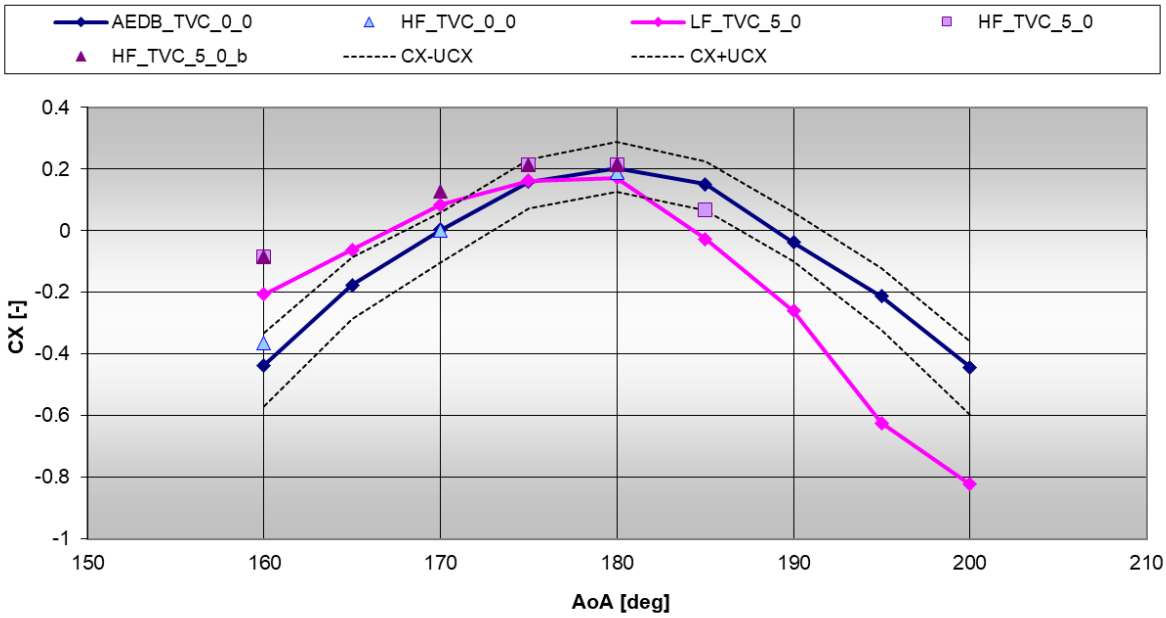

Figure 12: Impact of Thrust Vector Deflection on CX

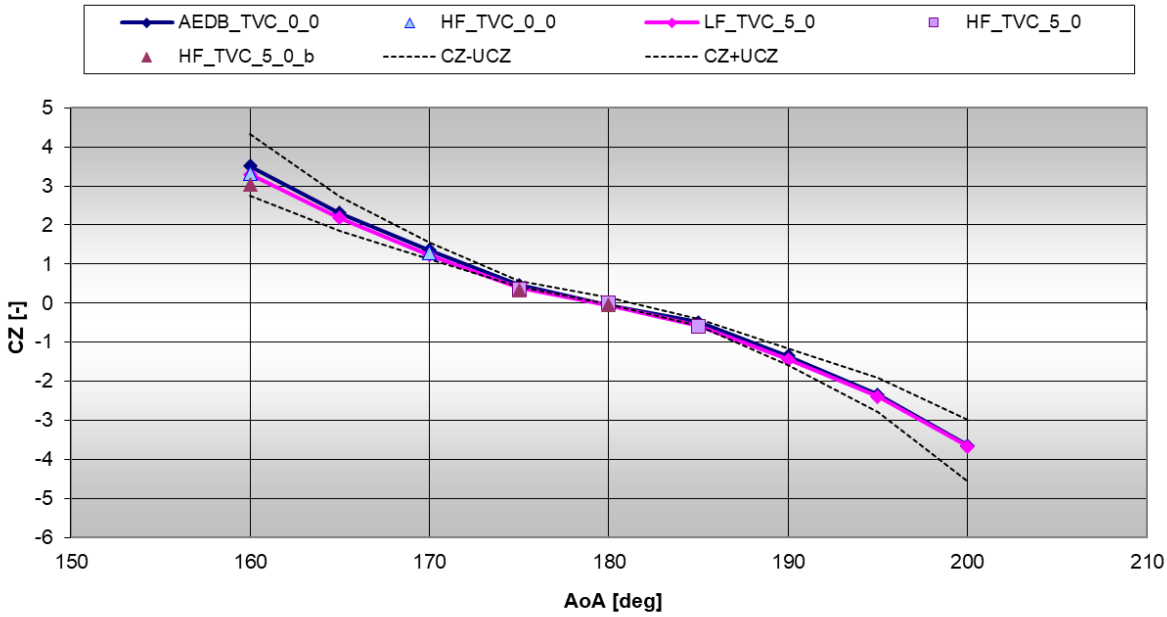

Figure 13: Impact of Thrust Vector Deflection on CZ.

The results show that the impact of the TVC deflection is especially significant for the axial force (CX-coefficient), whereas the impact on the normal coefficients (CZ or CY) is rather negligible and can be considered to be inside of the uncertainties of the SEDB.

The analysis of the flow pictures (Figure 11) allows a simplified physical interpretation: The flow changes due to the plume deflection are acting primarily on the base region of the vehicle, where the main part of the axial forces arises. The normal forces arise along of the whole vehicle and especially in the fin region while axial forces have a high contribution to the base area. Based on these findings the TVC-impact on the normal forces is not significant.

The proposed concept for considering the TVC-impact based on the idea of the local flow similarity assumption, e.g. the incident flow in the region of the base area is redirected by the engine jet (the engine plume imposes an effective

DOI: 10.13009/EUCASS2022-4689

flow conditions). The local effective angles φ_{eff}, and α_{eff} _eff are introduced. These angles can be easily calculated as the vector sum of the originally flow direction angles and TVC deflection.

$$CX = f(\varphi_{eff}, \alpha_{eff}; M); \quad \varphi_{eff}, \alpha_{eff} = f(\varphi, \alpha_s, M, TVC_q, TVC_r, \bar{\dot{m}})$$

where $\bar{\dot{m}}$ is the relative mass flow, M is Mach Number and TVC_q, TVC_r.are the TVC deflection angles for pitch and yaw control respectively.
The comparison presented in Figure 14 shows that CX-data calculated directly for the deflected TVC (magenta line) and CX-Data calculated by use of this concept (red line) are in reasonably good agreement for the reference flight point. The CX-Data originally prepared for the undeflected TVC are simply shifted for the corresponding φ_{eff}, and α_{eff} combination (Figure 14).

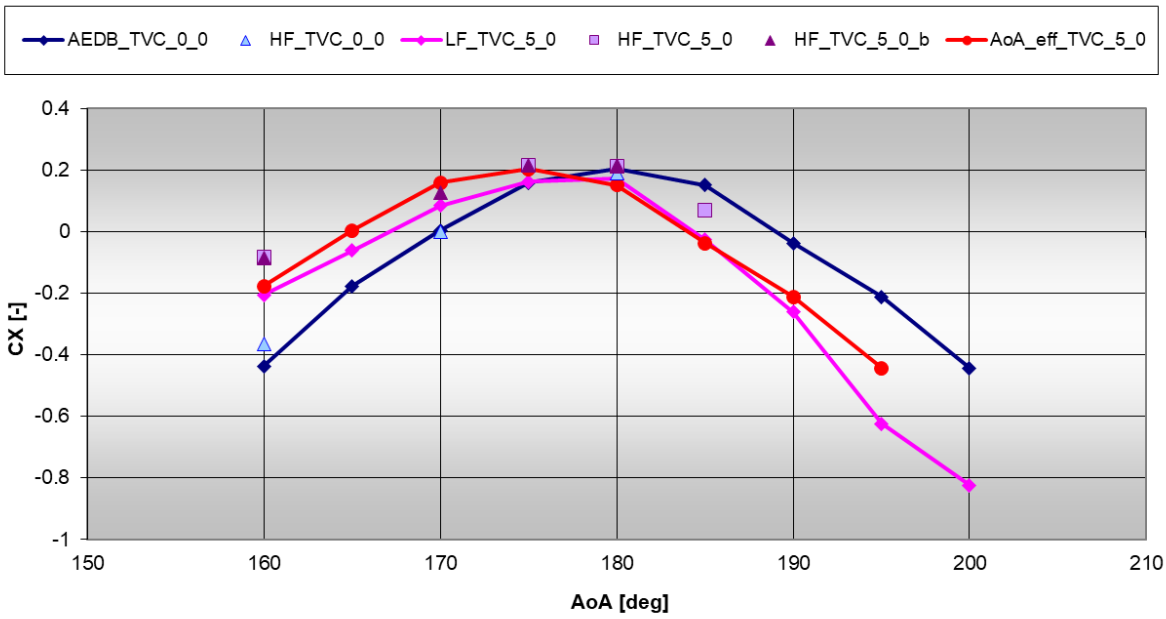

Figure 14: Considering of the TVC-Impact via AoA_eff

The advantages of this concept are:

- This concept can be easily generalized and is also applicable for the case, when AoA and TVC-deflections are not coplanar.
- No additional calculations are necessary and the existing AEDB can be used.

The drawbacks of this concept are:

- The shifting of the arguments for use with the existing databank constricts the AoA limitation for the use region: α_{eff} still should be kept inside of the allowed region, extrapolation of data is generally not recommended.
- Instationary effects are not considered.

Further checks showed that this method can be successfully applied to the UFO-configuration for all investigated flight Mach numbers M = 0.5 - 1.1. However, the use of this method cannot be recommended for UUO and FUO configurations: The interaction of the engine plume with the deployed legs makes the flow much more complex, and the TVC-impact cannot be reflected by simple arguments shift Phi_eff, Alpha_eff.
The TVC Impact on the normal forces (CY, CZ) can be neglected (Figure 13). For the axial force (CX) the uncertainties could be extended. In any case the UUO and FUO configuration are used for the flight phases by very low dynamic pressure q < 1000 Pa. Here, the aerodynamic forces are small: significantly smaller than the thrust and gravitation forces.

7. Uncertainties: Concept and Evaluation

The estimation of aerodynamic uncertainties mainly based on comparison of all available data: WTT (if available for the configuration) vs. CFD HR vs. CFD LR. This approach is exemplary illustrated by Figure 15.

DOI: 10.13009/EUCASS2022-4689

The main principle for application of the uncertainties is to keep the inner program module of the nominal aerodynamics unchanged if possible: The uncertainties will be considered outside of this program module before the input ("a priori") and after the output ("posteriori"). The primary uncertainties dependencies are listed below:

- Configuration: +
- Roll Angle: -
- Total Angle of Attack: +
- Mach Number: +
- Deflections: +-

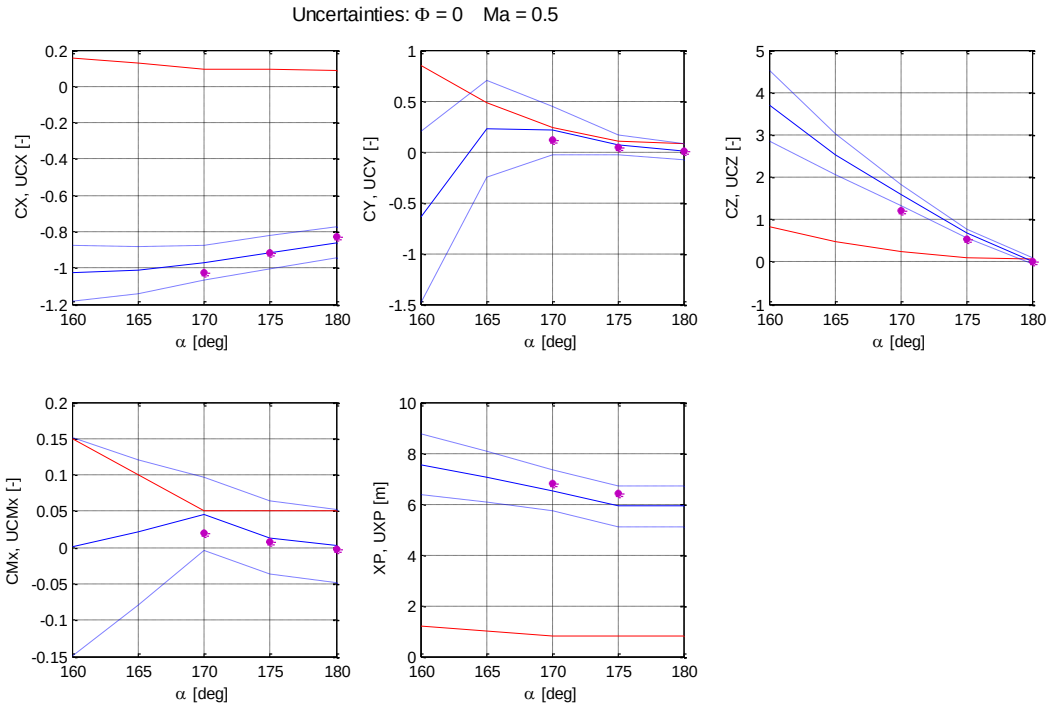

Figure 15: The nominal AEDB data and Uncertainties for UFN-configuration, M = 0.5, φ = 0°

Uncertainties estimation is primarily based on the comparison of:

- AEDB vs. High-Fidelity CFD (All Configuration, especially FFO, UFO, UUO)
- AEDB vs. WTT HST (UFN, FFN for Ma ≤ 1.3)
- AEDB vs. WTT TMK (UFN, FFN for Ma > 1.3)

The uncertainties terms are explained in Table 3

Table 3: Uncertainties Terms Explanation

Uncertainty Issue	**Uncertainty Term**	**Dependency**	**Note**
Forces Coefficients	[ΔCX,ΔCY,ΔCZ]T	f(Conf,φ,α_s,Ma)	Output Shift
Roll Coefficient	ΔCMx	f(Conf,φ,α_s,Ma)	Output Shift
Pitch and Yaw Coeff.	Impact will be introduced by Center of Pressure	f(Conf,φ,α_s,Ma)	Implemented indirectly
Center of Pressure	[ΔXcp,0,0]T	f(Conf,φ,α_s,Ma)	Input Shift, defined for δ = 0
Center of Mass	[ΔXcm,ΔYcm,ΔZcm]T	f(Conf, Fuel)	From MCI-Data
Damping Derivatives	Fω = diag{Fωx,Fωy,Fωz}	f(Conf,φ,α_s,Ma)	Input Factor

The application of uncertainties is schematically shown in Figure 16:

DOI: 10.13009/EUCASS2022-4689

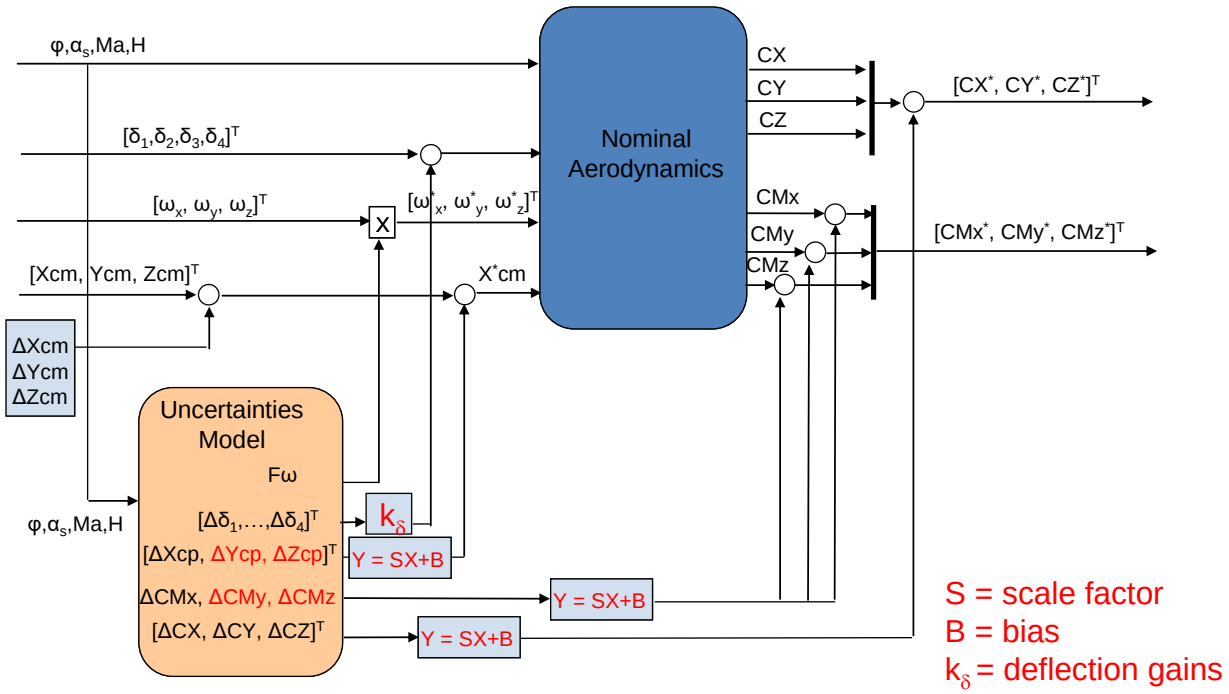

Figure 16: Uncertainties: Augmented Application Schema.

It is very important to reflect all physical relationships and dependencies between forces and moments, and it is particularly important to avoid the double consideration of uncertainties.

- Impact of the pitch and yaw moments uncertainties has been introduced by center of pressure shift (Variation ΔXcp).
- Impact of the of the fin / leg deflection uncertainties has been introduced by deflection shift and factor (Variation Δδi*).
- Impact of the damping uncertainties has been introduced by damping factors variation Fω:
- Impact of the roll moment and forces uncertainties has been introduced directly by shift (variation ΔCX, ΔCY, ΔCZ and ΔCMx):
- Impact of the pitch and yaw moments uncertainties has been introduced by center of pressure shift (variation ΔXcp, ΔYcp, ΔZcp):

8. Aerothermodynamic Aspects

Similar to the mechanical loads, aerothermal loads are a design driving factor during launcher development as the thermal loads impact thermal protection system during product design and trajectory optimisation. For the purpose of characterizing the aerothermal properties and loads of the CALLISTO vehicle aerothermal databases are generated periodically based on current aeroshape and flight domain. Due to the collaborative nature of the CALLISTO design process loads definition and respective thermal interfaces (tanks, legs, etc.) for the entire vehicle are defined. While the CAL1B aeroshape had 15 thermal interfaces, the number of interfaces for the CAL1C aeroshape has increased to more than 50 thermal interfaces due to is detailed description involving no symmetry and many of the final mechanical extensions (cable ducts, pipes, etc.). Compared to previous databases for the CAL1B shape, the extend of the CAL1C aerothermal database was tripled to 153 2D CFD calculations and more than 40 High-Fidelity 3D CFD while the number of grid points increased equally. The final CAL1C aerothermal database allows interpolation of interface heatfluxes for the entire flight domain at varying angle of attack (between 180° and 160°). More details can be found in references [16] and [17].

9. Conclusions

- The mission analysis allowed to define the primary and additional configuration necessary for AEDB.
- The proposed calculation philosophy has been applied by planning of the CFD-simulations and wind tunnel tests. More than 10000 Low-Fidelity CFD-simulations and hundreds of the High-Fidelity CFD-simulations were performed.
- The developed 'watertight' model of the vehicle reflected all the essential details of the considerably more complex aerodynamic shape. This model has been used both for the generation of the aerodynamic meshes for CFD simulation and served as the basis for the manufacturing of the aerodynamic models for the wind tunnel tests.
- The impact of the numerous design details on the aerodynamic performance compared to the ideal shape was evaluated and the measures for improving the aerodynamic shape have been proposed to reduce negative performance effects.
- The effective methods for performing the fin impact evaluation and distributed load calculation were applied.
- Another important aspect was the estimation of the uncertainties. Based on the comparison of results calculated by different CFD methods as well as experimental results obtained in different wind tunnels an uncertainty model has been developed and implemented in the flight simulator.
- The created AEDB allows the 6-DoF flight dynamics simulations necessary for the GNC development, including Monte-Carlo simulations.
- Especially the aerothermodynamic aspects play a very important role for a reusable vehicle. The created ATDB allows to estimate both the thermodynamic flux and integrated thermal loads during the reference mission, important data for the design of the thermal protection system.

References

[1] Dumont, E. et. al. (2021) *CALLISTO: A Demonstrator for Reusable Launcher Key Technologies.* Transactions of the Japan Society for Aeronautical and Space Sciences, Aerospace Technology Japan, JSASS 19 (1), pp. 106-115, 2021, DOI: 10.2322/tastj.19.106.

[2] Guedron, S. et. al. (2020) *CALLISTO DEMONSTRATOR: Focus on system aspects.* 71th International Astronautical Congress, 12.-14. October 2020, online. URL: https://elib.dlr.de/138808/

[3] Klevanski, J. and Ecker, T., Riehmer, J. and Reimann, B., Dumont, E., and Chavagnac, C. (2018) *Aerodynamic Studies in Preparation for CALLISTO - Reusable VTVL Launcher First Stage Demonstrator.* 69th International Astronautical Congress (IAC), 1-5 October 2018, Bremen, Germany. URL: https://elib.dlr.de/122062/

[4] Krummen, S. et al. (2021) *Towards a Reusable First Stage Demonstrator: CALLISTO - Technical Progresses & Challenges.* IAC-21-D2.6.1, 72nd International Astronautical Congress (IAC), 25.-29. October 2021, Dubai, UAE. URL: https://elib.dlr.de/147143/

[5] Marwege, A., Riehmer, J., Klevanski, J., Gülhan, A., Ecker, T., Reimann, B. and Dumont, E. (2019) *First Wind Tunnel Data of CALLISTO - Reusable VTVL Launcher First Stage Demonstrator.* EUCASS 2019, 1-4 July 2019, Madrid, Spain. URL: https://elib.dlr.de/128629/

[6] Marwege, A., Riehmer, J., Klevanski, J., Gülhan, A. and Dumont, E. (2019) *Wind Tunnel investigations in CALLISTO - Reusable VTVL Launcher First Stage Demonstrator.* 70th International Astronautical Congress (IAC), 21-25 October 2019, Washington D.C., United States. URL: https://elib.dlr.de/132566/

[7] Riehmer, J., Marwege, A., Klevanski, J., Gülhan, A. and Dumont, E. (2019) *Subsonic and Supersonic Groand Experiments for the CALLISTO VTVL Launcher Demonstrator*. International Conference on Flight Vehicles, Aerothermodynamics and Re-entry Missions & Engineering, 30 September – 3 October 2019, Monopoli, Italy. URL: https://elib.dlr.de/137501/

[8] Bhagat M. R., *SpaceX Falcon 9 v1.1, Falcon Heavy remodelling; Falcon 9 v1.1 descent trajectory and performance optimization*, SART TN-020/2014, 2014.

[9] *Blue Origin*, https://www.blueorigin.com/new-glenn, as accessed on September 15, 2017.

[10] Riehmer, J., Kapteijn, K. and Klevanski, J., Gülhan, A. and Dumont, E. (2022) *Wind Tunnel Experiments of the CALLISTO VTVL Launcher in the TMK and HST Wind Tunnels.* EUCASS 2020, 27.06-01.07.2022, Lille, France.

[11] Ecker, T., Ertl, M., Klevanksi, J., Krummen, S. and Dumont E. (2022). *Aerothermal characterization of the CALLISTO vehicle during descent*. EUCASS 2020, 27.06-01.07.2022, Lille, France.

[12] William B. Blake (1998): *Missile DATCOM User's Manual* - 1997 FORTRAN 90 Revision. Air Vehicles Directorate, Air Force Research Laboratory, Air Force Materiel Command Wright Patterson Air Force Base, Ohio 45433-7562.

DOI: 10.13009/EUCASS2022-4689

[13] Langer, S. and Schwöppe, A. and Kroll, N. (2014) *The DLR Flow Solver TAU - Status and Recent Algorithmic Developments*. 52nd Aerospace Sciences Meeting, 13-17 January 2014, National Harbor, Maryland, USA.
[14] CentaurSoft, http://www.centaursoft.com
[15] Spalart, P. R., Allmaras, S. R., *A One-Equation Turbulence Model for Aerodynamic Flows*, AIAA-92-0439, 30th Aerospace Sciences Meeting and Exhibit, Reno, USA, 1992, 6-9 January. DOI: 10.2514/6.1992-439.
[16] T. Ecker, M. Ertl, J. Klevanski, S. Krummen and E. Dumont,. Aerothermal characterization of the callisto vehicle during descent. In 9th European Conference for Aeronautics and Space Sciences, 2022.
[17] M. Ertl, T. Ecker, J. Klevanski, E. Dumont, and S. Krummen. "Aerothermal analysis of plume interaction with deployed landing legs of the CALLISTO vehicle". In: 9th European Conference for Aeronautics and Space Sciences. 2022.